



ELSEVIER

Fluid Dynamics Research 29 (2001) 295–311

**FLUID DYNAMICS  
RESEARCH**

## Regular and chaotic streamlines of two vortex rings

Emily S.C. Ching<sup>a</sup>, Yongnian Huang<sup>a,b</sup>, Norbert Schorghofer<sup>a,\*</sup>

<sup>a</sup>*Department of Physics, The Chinese University of Hong Kong, Shatin, Hong Kong*

<sup>b</sup>*Department of Mechanics and Engineering Science, State Key Laboratory of Turbulence Research, Peking University, Beijing 100871, People's Republic of China*

Received 31 January 2001; received in revised form 6 June 2001; accepted 6 August 2001

---

### Abstract

We study the streamlines of the velocity field generated by two Helmholtz vortex rings which are fixed in space. Chaos can arise directly from a perturbation of periodic orbits. Trajectories are regular far away from linked vortex rings, and chaotic far away from unlinked vortex rings. Intersections of vortex rings produce intricate streamline topologies. The correspondence between the topology of the streamlines and the topology of the vortex rings is discussed. © 2001 Published by The Japan Society of Fluid Mechanics and Elsevier Science B.V. All rights reserved.

*PACS:* 47.52.+j; 47.32.Cc; 05.45.Ac

*Keywords:* Vortex ring; Streamline topology; Chaotic advection

---

### 1. Introduction

Vortex rings appear in innumerable applications and can be reproduced in laboratory experiments (Lugt, 1983; Shariff and Leonard, 1992). Coherent vortex structures have also been identified in various turbulent flows (Vincent and Meneguzzi, 1991; Jimenez et al., 1993; Belin et al., 1996). This led to the hope of modeling complex turbulent flows by vortex systems. Promising attempts have been made to obtain statistical characteristics of turbulence from a random arrangement of Burgers vortices (Hatakeyama and Kambe, 1997; He et al., 1999; Kambe and Hatakeyama, 2000). For three-dimensional turbulence the typical localized vortex has the topology of a ring. It is hence of considerable interest to study the flow induced by vortex ring structures.

There has been a large amount of research on two-dimensional point vortices (Aref, 1983) and vortex rings (Shariff and Leonard, 1992). Besides studying the dynamics of vortex systems, it is also of interest to study the generated flow field and the advection of passive tracer particles (Stone et al.,

---

\* Corresponding author. Current address: Department of Earth, Atmospheric, and Planetary Sciences, Massachusetts Institute of Technology, Room 54-627, Cambridge, MA 02139, USA. Tel.: +1 (617)2537278; fax: +1 (617)2531699.  
*E-mail address:* norbert@segovia.mit.edu (N. Schorghofer).

1991; Shi et al. 1992; Pentek et al., 1996; Neishtadt et al., 1998; Kroujiline and Stone, 1999; Kidambi and Newton 2000; Domon et al., 2000). In particular, the motion of the passive tracer particles may be chaotic even when the vortex dynamics is regular. Relatively little work has been done on the streamlines of three-dimensional vortex systems.

In the present work, we study the three-dimensional incompressible velocity field generated by two Helmholtz vortex rings. The well-known Helmholtz vortex ring solution is a circular vortex ring with infinitely small core. As a first study, we ignore the influence of one vortex ring by the velocity field of the other and consider the vortex rings to be fixed in space. Thus, the velocity field is time-independent and as a result, the trajectories of the advected passive tracer particles coincide with the streamlines of the velocity field. Our results can also be understood as the streamlines of the velocity field at the initial instant before the rings start to move under the influence of the other ring. As the rings move, they are likely to be deformed. It is plausible that more general closed vortex structures retain characteristics of the flow field of the simpler problem studied here, which is numerically and analytically far more tractable.

Highly symmetric ring configurations, where the axes of the two rings lie on the same plane, are systematically treated by the authors in Huang et al. (2000). Detailed conditions for the integrability of streamlines are discussed there. The present work is primarily concerned with ring orientations that induce chaotic flows, which is the generic situation for a two-ring configuration. The flow exhibits a rich spatial structure, which we devote this study to. Our analysis involves conventional methods of dynamical system theory. For application of such methods to fluid dynamics see Perry and Chong (1987) and Arnold and Khesin (1998).

Section 2 introduces the vortex ring model. The following four sections are organized according to the topological arrangement of the two rings. Motion around two rings with a common center (Section 3) is integrable, though not simple at all. Linked vortex rings are discussed in Section 4. The special stage with one vortex ring intersection is treated in Section 5, and finally the unlinked configuration is described in Section 6. The final section contains a summary and further discussion.

## 2. Setup

Because of the axial symmetry of the geometry, the velocity field of a Helmholtz vortex ring can be expressed in terms of a stream function  $\psi$ . For a vortex ring of radius  $a$  and strength  $\kappa$ ,  $\psi$  is given by (Lamb, 1932)

$$\psi(x, r) = \frac{\kappa}{2\pi} \sqrt{ar} \left[ \left( \frac{2}{k} - k \right) \mathbf{K}(k) - \frac{2}{k} \mathbf{E}(k) \right] \quad (1)$$

with  $k^2 = 4ar/[x^2 + (r + a)^2]$ , where  $r$  is the distance from the axis of the ring and  $x$  the distance from the plane of the ring. The expression contains the complete elliptic integrals  $\mathbf{K}(k) = \int_0^{\pi/2} 1/\sqrt{1 - k^2 \sin^2 \theta} d\theta$  and  $\mathbf{E}(k) = \int_0^{\pi/2} \sqrt{1 - k^2 \sin^2 \theta} d\theta$ . From the stream function one can work out the radial and axial velocity components

$$-u_r = \frac{1}{r} \frac{\partial \psi}{\partial x} = \frac{\kappa}{4\pi} \frac{x}{r} \frac{1}{\sqrt{x^2 + (r + a)^2}} \left[ \mathbf{E}(k) \frac{k^2 - 2}{1 - k^2} + 2\mathbf{K}(k) \right], \quad (2a)$$

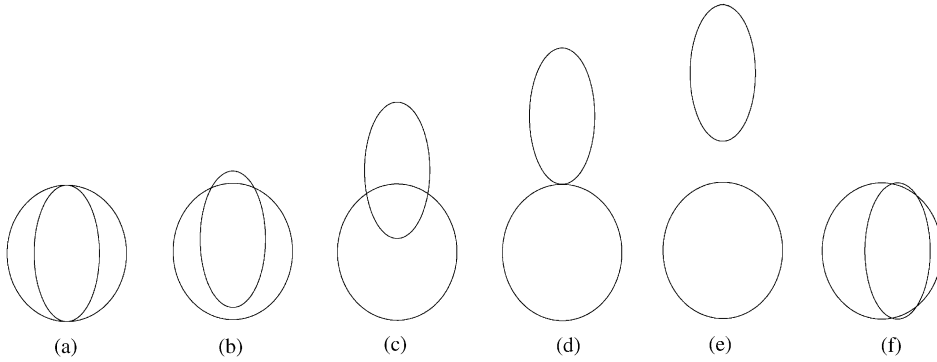


Fig. 1. Overview of vortex ring configurations shown in this paper. The vertical axis is  $x_3$ . (a) common center, Figs. 2–4. (b) linked, Fig. 5. (c) linked, Fig. 6. (d) one intersection, Figs. 7, 8. (e) unlinked, Figs. 9 and 10 (actual separation is larger than shown). (f) unlinked, Fig. 11.

$$u_x = \frac{1}{r} \frac{\partial \psi}{\partial r} = \frac{\kappa}{4\pi} \frac{1}{\sqrt{x^2 + (r+a)^2}} \left[ \mathbf{E}(k) \frac{k^2(1+a/r) - 2}{1-k^2} + 2\mathbf{K}(k) \right]. \tag{2b}$$

Since the velocity is irrotational everywhere except on the vortex ring,  $\psi$  satisfies the following equation:

$$\frac{\partial^2 \psi}{\partial x^2} + \frac{\partial^2 \psi}{\partial r^2} - \frac{1}{r} \frac{\partial \psi}{\partial r} = 0. \tag{3}$$

As a result of the linearity of Eq. (3), multiple ring solutions can be obtained by superposition.

Throughout the paper, we study two vortex rings with the following configuration. Both rings have equal radius  $a = 1$  and strength  $\kappa = 2$ . The first vortex ring has its axis along the  $x_1$ -axis, the second along the  $x_2$ -axis. Hence the two rings are perpendicular to one another. Except in one configuration, which will be pointed out, the centers are located along the  $x_3$ -axis at coordinates  $(0, 0, -d)$  and  $(0, 0, d)$  so that the ring centers are separated by a distance of  $2d$ . Several of the ring configurations we have investigated are illustrated in Fig. 1.

The velocity field of our two vortex rings becomes

$$u_1 = + \frac{1}{r_1} \frac{\partial \psi_1}{\partial r_1} - \frac{x_1}{r_2^2} \frac{\partial \psi_2}{\partial x_2}, \tag{4a}$$

$$u_2 = - \frac{x_2}{r_1^2} \frac{\partial \psi_1}{\partial x_1} + \frac{1}{r_2} \frac{\partial \psi_2}{\partial r_2}, \tag{4b}$$

$$u_3 = - \frac{x_3 + d}{r_1^2} \frac{\partial \psi_1}{\partial x_1} - \frac{x_3 - d}{r_2^2} \frac{\partial \psi_2}{\partial x_2}, \tag{4c}$$

where  $\psi_1 = \psi(x_1, r_1)$  with  $r_1^2 = x_2^2 + (x_3 + d)^2$  and  $\psi_2 = \psi(x_2, r_2)$  with  $r_2^2 = x_1^2 + (x_3 - d)^2$ . To evaluate the streamlines, we numerically (Press et al., 1992) solve the differential equations:

$$\frac{dx_i}{dt} = u_i, \quad i = 1, 2, 3. \tag{5}$$

The expression for the velocities can be cast in different forms. The form most suitable for numerical evaluation is in terms of elliptic integrals which is the form given in Eq. (1). The divergence in Eqs. (2a) and (2b) for  $k \rightarrow 1$  corresponds to the physical divergence of the velocity field close to the ring. A potential numerical problem occurs close to the axis of the vortex ring ( $r \rightarrow 0$ ), since in this limit the two terms with the elliptic integrals cancel each other and, despite vanishing denominator, the velocity remains finite. A remedy is readily found. The velocity along  $r = 0$  can be obtained in closed form and an expansion in the neighborhood suffices to guarantee accuracy even in this region of space. For  $r \ll a$  one obtains

$$u_x = \frac{\kappa}{2} \frac{a^2}{(x^2 + a^2)^{3/2}} + O(r^2), \quad (6a)$$

$$-u_r = \frac{3\kappa}{4} \frac{xra^2}{(x^2 + a^2)^{5/2}} + O(r^2). \quad (6b)$$

Simple error considerations show that these formulas should be used when  $r^3 < O(\varepsilon)$ , where  $\varepsilon$  is the error of the elliptic function evaluation. For our calculations  $r < 10^{-5}$ , so that the region in question occupies only a tiny fraction of volume. Elliptic integrals can be quickly evaluated to high accuracy (Moshier, 1992). The dominant error then lies in the integration of the differential equations (5), and this accuracy can be varied to check the dependence on numerical errors. In conclusion, numerics can be done with great reliability and speed.

As a last preliminary we consider general properties of fixed (stagnation) points ( $\vec{u} = 0$ ). For an irrotational fluid the stability matrix is real and symmetric, and hence has three real eigenvalues. In an incompressible flow the three eigenvalues add up to zero. Fixed points are hence always hyperbolic. Only when a fixed point coincides with a vortex ring can it possess complex eigenvalues and act as a focus or center.

### 3. Vortex rings with common center

We start with the simple situation where the vortex rings share the same center ( $d = 0$ ) and consequently intersect each other twice. In this case all of the trajectories are periodic, that means they are closed orbits. According to our simulations two types of motion occur. Both types of trajectories are shown in Fig. 2. One type of motion is a periodic orbit encircling both vortex rings at once. The other type of trajectories wind around one ring for a while and hops eventually over to the other ring. The resulting orbit is periodic with two frequencies. There is no motion around one vortex ring only, nor are there any chaotic trajectories. We shall explain this behavior in the following.

In this highly symmetric situation there are two invariant planes dividing the space into four independent parts. One invariant plane is  $x_3 = 0$ , the other  $x_1 = x_2$  (M-plane). Both are also symmetry planes and streamlines repeatedly intersecting the M-plane must therefore be periodic (Huang et al., 2000). Further, there is a line of fixed points lying in the  $x_1 = -x_2$  plane (N-plane). From Eqs. (4a)–(4c) and (2a, 2b) one obtains after a straightforward calculation the condition for a fixed point

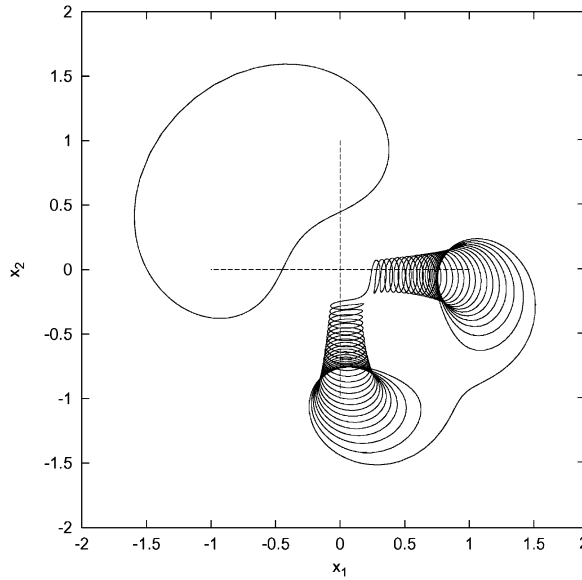


Fig. 2. The two possible types of trajectories for  $d = 0$ , projected onto the  $x_3 = 0$  plane. The vortex rings are drawn with dashed lines.

Table 1

Various positions of fixed points for  $d = 0$  among an infinity of such points. Fixed points are located at  $(x, -x, x_3)$ ,  $(-x, x, x_3)$ ,  $(x, -x, -x_3)$  and  $(-x, x, -x_3)$

$x_3$	$x$ (approx.)
0	0.885
0.09	0.882
0.6	0.738
0.9	0.467
1	0.161 and 0
1.001	0.144 and 0.038
> 1.01	—

at  $(x, -x, x_3)$ :

$$\left[ 2 - k^2 \left( 1 + \frac{ar}{r^2 + x^2} \right) \right] \mathbf{E}(k) = 2(1 - k^2)\mathbf{K}(k) \tag{7}$$

with  $k^2 = 4ar/[x^2 + (r + a)^2]$  and  $r^2 = x^2 + x_3^2$ . Several numerically obtained solutions to this equation are shown in Table 1. The line of fixed points reaches from one intersection of the vortex rings to the other and back, forming an oval curve.

A fluid element encircling one ring feels a velocity component from the other ring and it drifts either towards the intersection of the two rings or towards the invariant  $x_3 = 0$  plane. In an

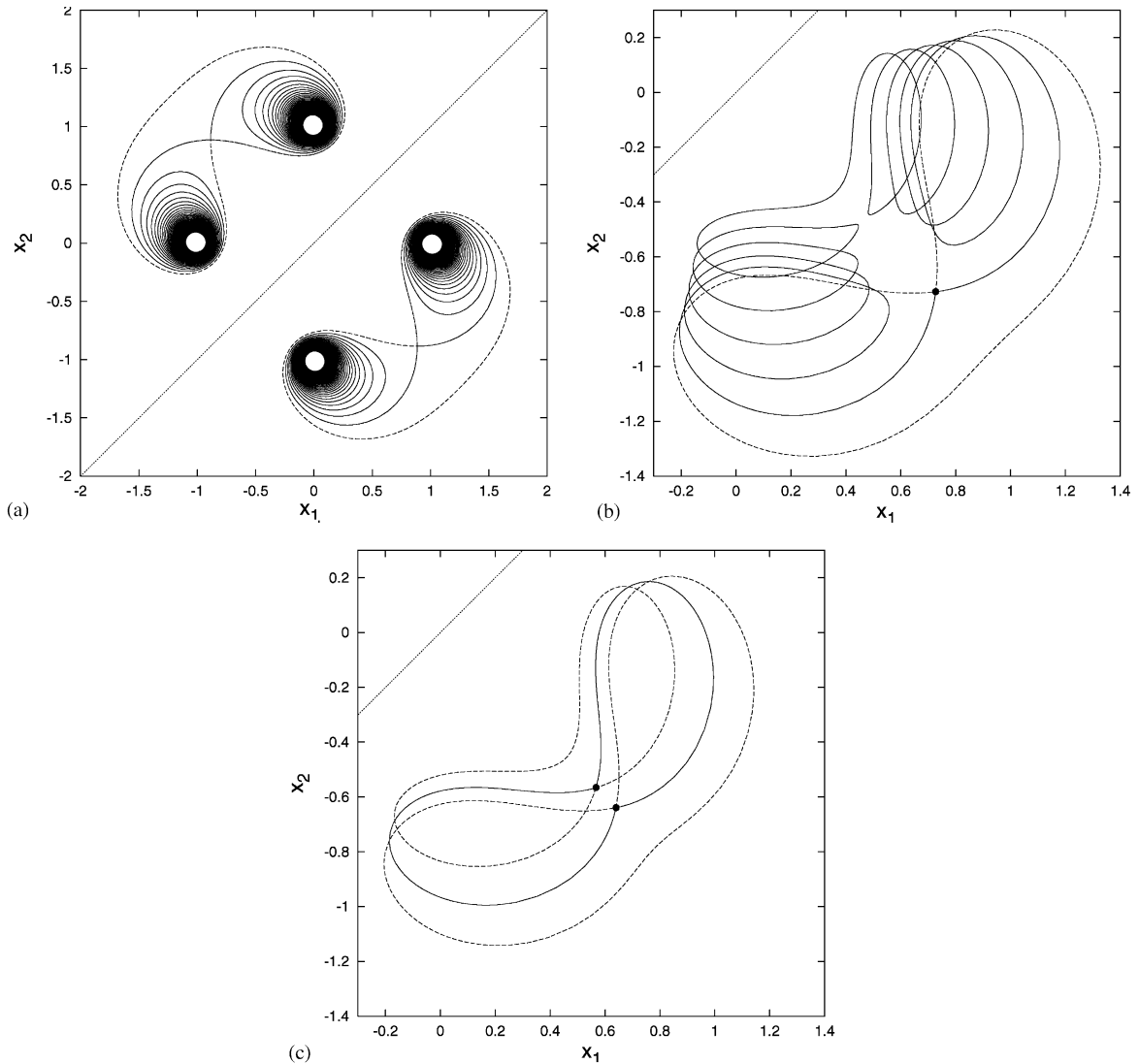


Fig. 3. Invariant manifolds for  $d=0$  (solid, dashed and dotted lines). The manifolds are visualized by integrating a trajectory starting very close to the fixed point forward and backward in time. (a) Invariant manifolds on the  $x_3=0$  plane. The vortex rings go through the four white spots, which are only left white because of finite integration time. Two hyperbolic fixed points can be seen. (b) An invariant manifold outside the  $x_3=0$  plane (projection). It consists of one hyperbolic fixed point (marked with  $\bullet$ ) and two homoclinic cycles, one of which is drawn with dashed lines for clearer distinction. (c) A special invariant manifold outside the  $x_3=0$  plane (projection). It has two hyperbolic fixed points (marked with  $\bullet$ ) that are connected by two homoclinic cycles (dashed lines) and two heteroclinic cycles (solid lines). This particular manifold shows how the fixed line changes from the inner to the outer side of the “double-cone”.

incompressible flow it can however never reach either of them and it jumps onto the other ring to drift backward. What structure of invariant manifolds allows for such nested jumps back and forth?

Fig. 3a shows fixed points and stable and unstable invariant manifolds on the  $x_3=0$  plane. The vortex rings act in this specific situation as sources and sinks of streamlines. This is possible despite

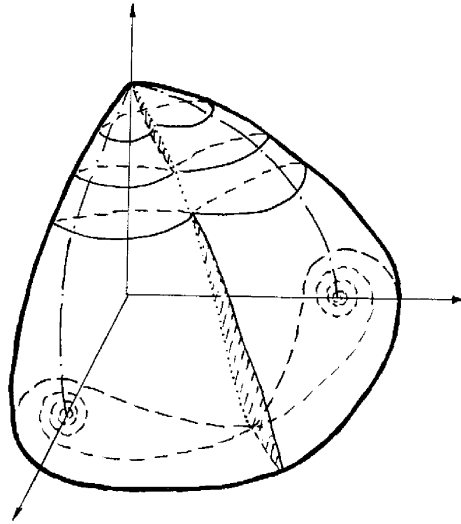


Fig. 4. Schematic drawing of the “double-cone” surface that separates the two types of streamlines. The dash-dot lines are segments of vortex rings. The shaded cross-section shows how the line of fixed points (dotted line) passes from the inner to the outer side of the double-cone.

the incompressibility of the flow, because the two-dimensional divergence of the velocity field in this plane does not vanish. Away from the  $x_3 = 0$  plane, the topological structure is more intricate. Fig. 3b shows an invariant manifold consisting of two homoclinic cycles and a fixed point. Fig. 3c shows one of many special invariant manifolds that have two fixed points and form a heteroclinic cycle and two homoclinic cycles. Nearby manifolds have only one fixed point, no heteroclinic cycles, and one winding fewer or more. Invariant manifolds with two fixed points, such as in Fig. 3c, separate families of manifolds with one fixed point, such as in Fig. 3b. There are infinitely many manifolds of each kind. In Fig. 3b one sees the manifold intersects the N-plane once inside and once outside of the line of fixed points. Fig. 3c shows exactly how this transition happens. This allows streamlines to coil upwards on one ring, move over to the other, coil downwards, and finally return to their original starting point.

The separatrix of the two types of trajectories is topologically equivalent to a double-cone with its top at the intersection of the vortex rings and its base on the  $x_3 = 0$  plane (see Fig. 4). There are two cones connected to each other. Somewhere in the middle, the cone is squeezed to touch the other side, but the volume within remains connected. By symmetry each of the four independent quarters of space has one such double cone.

#### 4. Linked vortex rings

For  $0 < d < 1$  the two vortex rings are linked with each other and have no common intersection. There are three types of trajectories (streamlines): periodic, quasi-periodic and chaotic. Streamlines can wind around only one ring, both rings at once, or jump back and forth the two rings in a chaotic

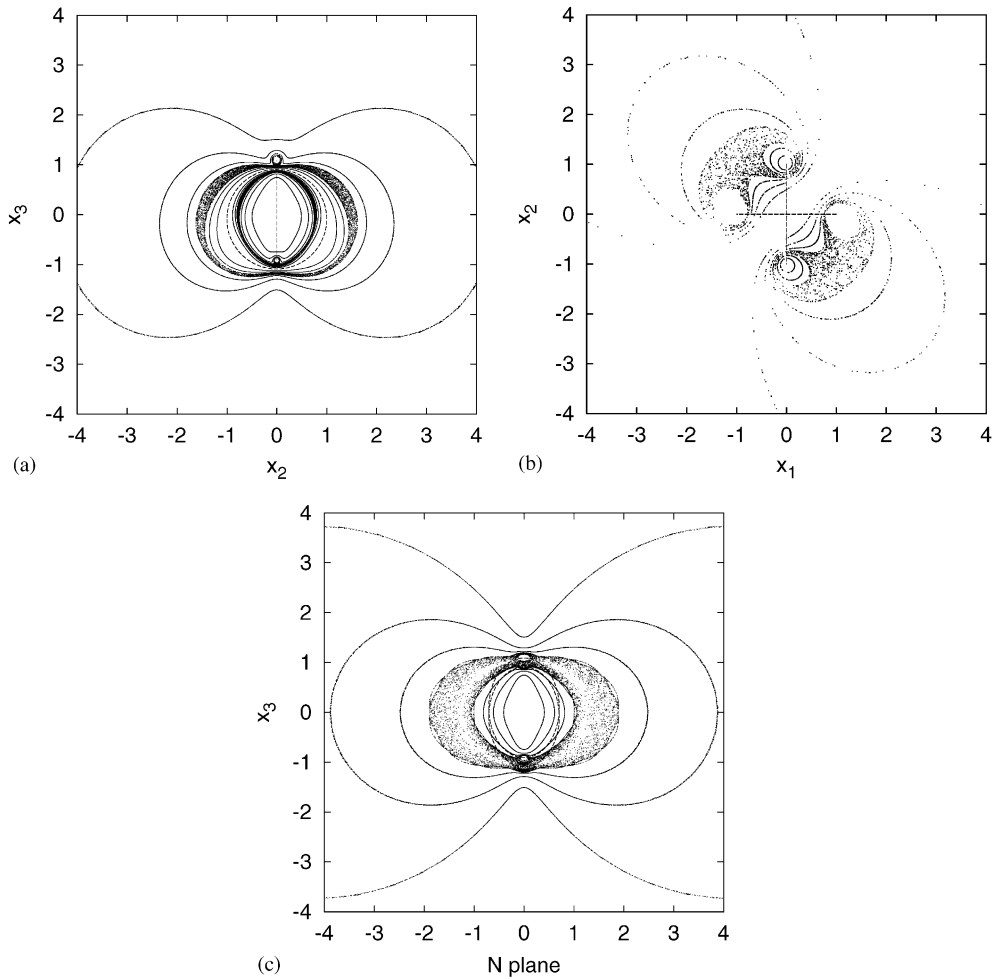


Fig. 5. Poincaré sections for  $d=0.09$ . The vortex rings are drawn with dashed lines. Quasi-periodic and chaotic regions are clearly seen. In part (c) regular islands are discernible at the boundary between regular and chaotic region.

manner. Fig. 5 shows Poincaré sections for various initial conditions when  $d=0.09$ . Streamlines encircling one ring form a torus of quasi-periodic orbits. Streamlines encircling both rings with one turn also drift along, forming large tori of quasi-periodic motion. All motion far from the vortex rings evolves on such tori and is hence regular.

A separation of  $d=0.09$  may be considered a perturbation of the  $d=0$  configuration. Comparison of Fig. 3a with Fig. 5b shows that the trajectories which for  $d=0$  spiral up and down both rings transform into chaotic trajectories and trajectories that encircle only one ring. It is the breakdown of the complex manifold structure within the double-cone, discussed in the previous section, which leads to chaos. The closed line of fixed points is destroyed, so are the many homoclinic and heteroclinic cycles. The transition to chaos happens from periodic orbits to chaos directly through a global bifurcation (Wiggins, 1988).

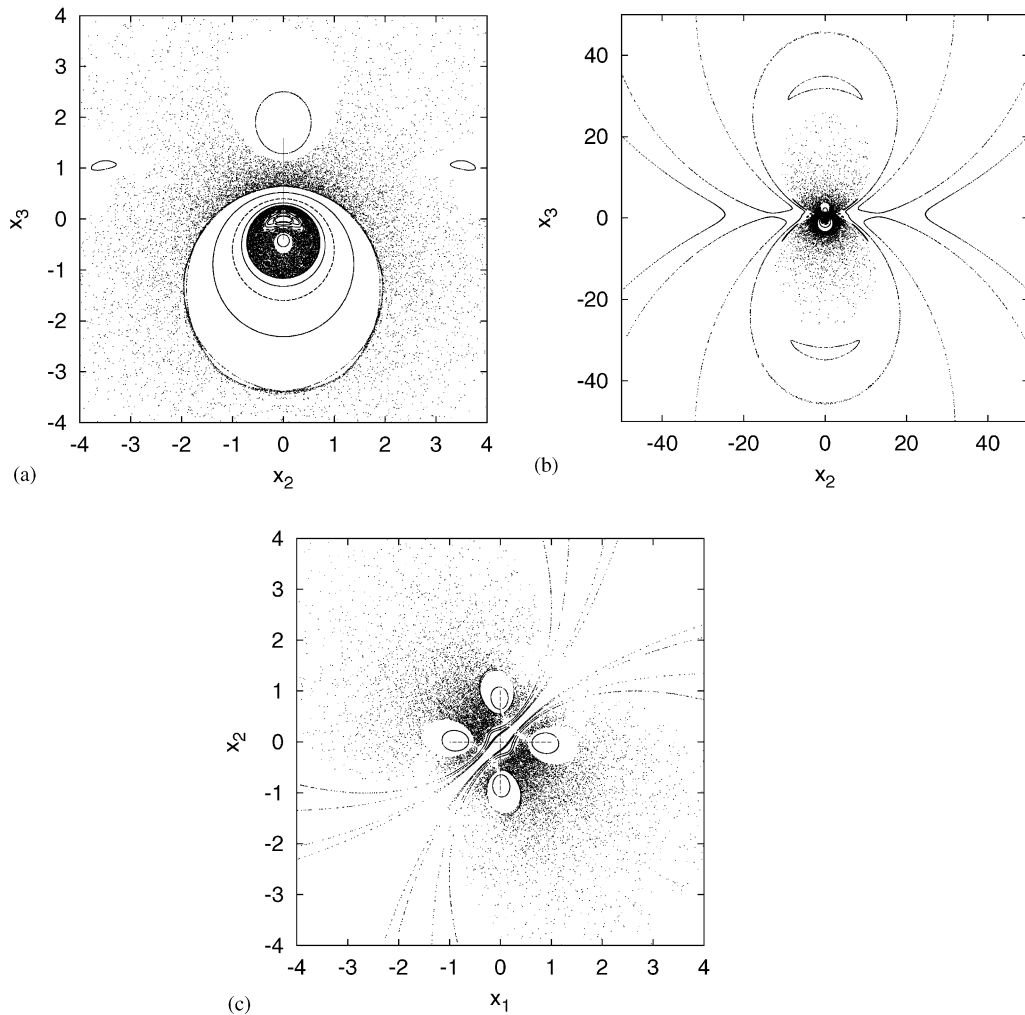


Fig. 6. Poincaré sections for  $d = 0.6$ . Shown are small tori, chaotic motion, and giant outer tori in addition to other regular structures. The chaotic region is large, but does not extend to infinity.

Numerical searches for equilibrium points in the entire space, using a Newton–Raphson method (Press et al., 1992), did not turn up any remaining fixed points. Hence, the chaotic region is apparently created by the stable and unstable manifolds of unstable periodic orbits.

The chaotic and regular regions are much like one would expect for a conservative system. Regular islands and stochastic layers appear at the boundary regions. The chaotic region grows with the perturbation parameter. In fact as  $d$  increases from zero, the chaotic region appears in the double-cone first, then gradually extends in size inward as well as outward.

We find that any situation with  $0 < d < 1$  is qualitatively similar, as one would expect from topological equivalence. Fig. 6 shows one more linked configuration,  $d = 0.6$ . The chaotic region is

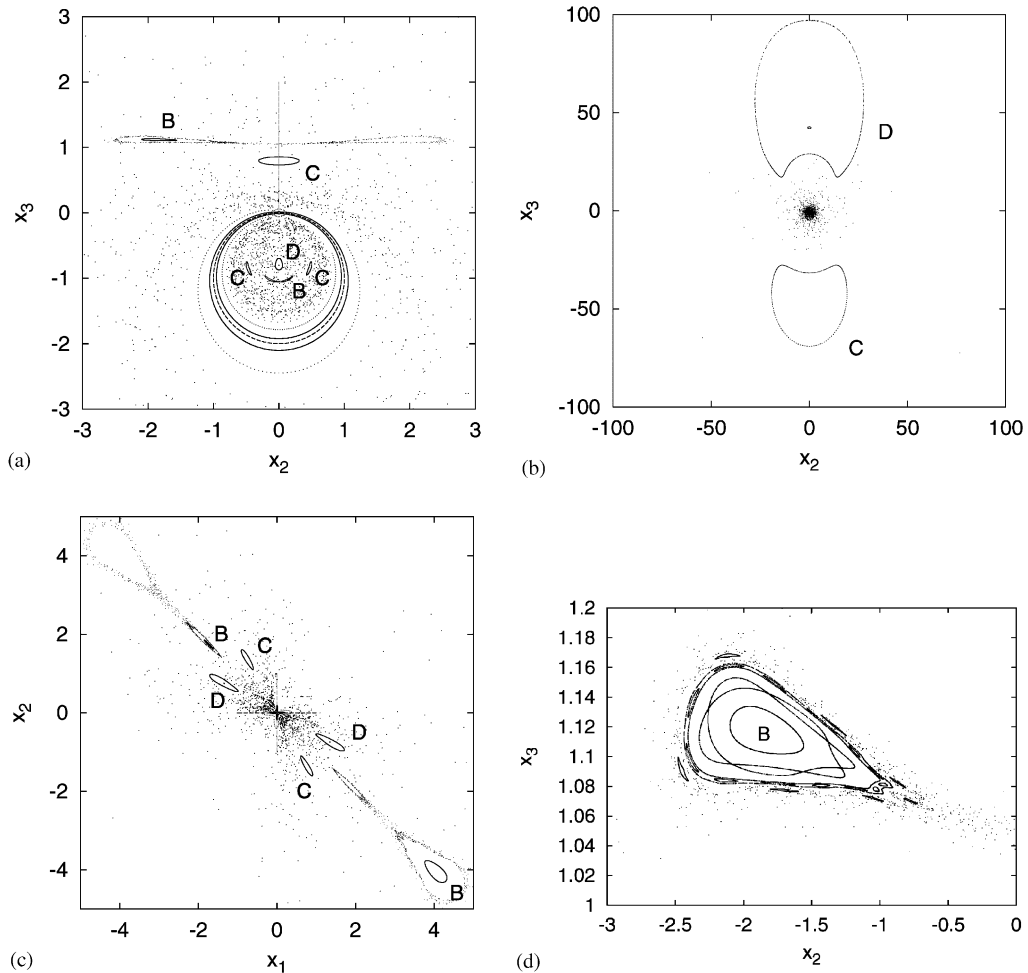


Fig. 7. Poincaré sections for  $d=1$ . The tori labeled B and D wind around both vortex rings at once, while torus C winds around the first ring twice as often than around the second ring. The location of the B torus within its surrounding chaotic structure reveals, in parts (a) and (c), a twist in the structure. An enlarged view of this eight-figure structure is shown in part (d), using different initial conditions and distorting aspect ratio. Such structures are typical for conservative chaotic systems. We have observed similar structures also for  $d \neq 1$ .

extended in size but still bounded. This leads to the conclusion that chaotic streamlines of linked vortex rings never extend to infinity.

## 5. Vortex rings with one intersection

When  $d=1$ , the two rings intersect each other once. This is a degenerate and the most complex case. Poincaré sections for  $d=1$  are shown in Fig. 7. The behavior is chaotic throughout and without major invariant surfaces. For  $d < 1$  the hole of a huge outer torus goes through both vortex rings,

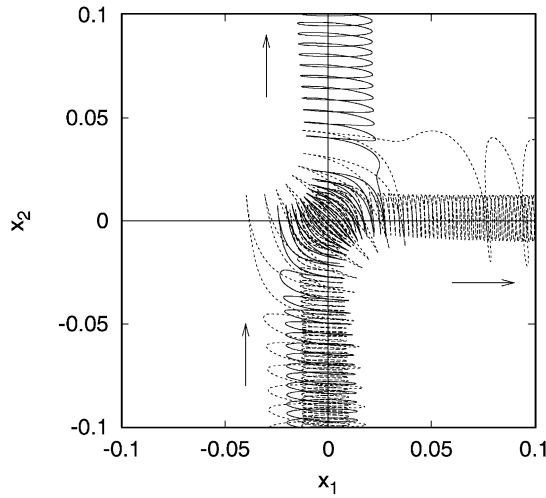


Fig. 8. Three streamlines (solid, dashed, dotted) close to the intersection of the vortex rings (thick solid lines). At some stage they wind around both rings and can end up on either ring. The (solid) streamline with a distance from the ring intermediate between the other two trajectories (dashed, dotted) returns to the same ring it started from, while the other two change to the other ring. This illustrates part of the nested manifold structure. Arrows indicate whether the trajectories drift towards or away from the intersection.

such that the torus contains both vortex rings in its interior. For  $d = 1$  this is no longer possible. Chaotic streamlines extend to infinity.

In the remainder of this section we study the behavior close to the ring intersection. In Section 3 we have observed a complex topological structure of stable and unstable invariant manifolds for  $d = 0$ . Here,  $d = 1$ , the intersection of vortex rings also involves intricate structures.

Fig. 8 shows three trajectories close to the intersection. They move through the intersection and hop either onto the other ring or back onto the ring they started from. The distribution of initial conditions that go one or the other way consists of a large number of twined layers. Further investigation shows that the layers have finite thickness, meaning that a single passage through the intersection generally does not separate nearby initial conditions. Trajectories such as those shown in Fig. 8 wind around the ring many times before they return to the intersection. Each different number of windings is topologically distinct. It appears that these trajectories are chaotic, but we have not studied their properties in more detail.

As a mere check, one can work out an approximation to the velocity field close to the intersection  $|\vec{x}| \ll a$ . One obtains

$$u_1 = -\frac{\kappa}{2\pi} \frac{x_3}{x_1^2 + x_3^2} + O(\log|\vec{x}|), \tag{8a}$$

$$u_2 = +\frac{\kappa}{2\pi} \frac{x_3}{x_2^2 + x_3^2} + O(\log|\vec{x}|), \tag{8b}$$

$$u_3 = \frac{\kappa}{2\pi} \left( \frac{x_1}{x_1^2 + x_3^2} - \frac{x_2}{x_2^2 + x_3^2} \right) + O(1). \tag{8c}$$

Since the velocity is singular at this point, this approximation does not capture the behavior in all directions of space, but it must capture some of the behavior in the neighborhood. From Eqs. (8a)–(8c) we obtain  $\vec{u} \cdot \vec{x} = 0$ . Hence  $x_1^2 + x_2^2 + x_3^2 \equiv R^2 = \text{const}$ . Therefore, trajectories move on a sphere with radius  $R$ . Dividing the first two components by one another and integrating yields a second invariant of motion

$$\frac{(R + x_1)(R + x_2)}{(R - x_1)(R - x_2)} = \text{const}. \quad (9)$$

Therefore, there are periodic orbits on the N-plane ( $x_1 = -x_2$ ) and fixed points along the line  $x_1 = x_2, x_3 = 0$ . The truncated equations (8a)–(8c) correctly produce trajectories that wind around the  $x_1 = x_2, x_3 = 0$  axis. A trajectory could however, in this approximation, never pass through the N-plane. The next order in the expansion contains a logarithmically small sweep velocity that accounts for the passage through the intersection in finite time.

## 6. Unlinked vortex rings

Unlinked vortex rings ( $d > 1$ ) typically have chaotic streamlines. Fig. 9 shows Poincare sections for  $d = 2.13$ . A sharp borderline between chaotic regions appears, in addition to several regular structures. A chaotic streamline in one region is never observed in the other region. (This could be seen from Fig. 9, if every initial condition were drawn in a different color. The border becomes indirectly visible in this figure, because the density of points in the Poincare section is different in the two regions.) Consequently a surface must exist that separates space into two parts, each containing chaotic streamlines.

Again, we start our understanding of the topology with an analysis of invariant sets. The line  $x_3 = 0, x_1 = x_2$  is invariant for any  $d$ . Using Eqs. (4a)–(4c) and (2a, 2b), the condition for a fixed point on this line is:

$$\left[ 2 - k^2 \left( 1 + \frac{ar}{d^2} \right) \right] \mathbf{E}(k) = 2(1 - k^2) \mathbf{K}(k) \quad (10)$$

with  $k^2 = 4ar/[x^2 + (r + a)^2]$  and  $r^2 = x^2 + d^2$ . From the sign of the first term in brackets it is readily shown that this equation can only have solutions for  $d \geq a$ . Table 2 lists several fixed point solutions.

In Fig. 9 the fixed points lie on the boundary between chaotic regions. At the intersections of the invariant surface with the vortex rings, the velocity exerted by the other ring is perpendicular to the vortex ring. The separating surface has the topology of a sphere. The eigendirections of the fixed points on the separating surface can be calculated numerically and are used to visualize the stable and unstable manifolds in Fig. 10. The two fixed points are hyperbolic within the surface and the vortex rings act as foci. Each of the two hyperbolic fixed points is connected with the vortex rings by heteroclinic orbits. This splits the surface into four parts. All streamlines on this manifold are heteroclinic trajectories connecting different singularities and fixed points.

Now we turn to the regular structures seen in Fig. 9. Most notably there is a torus within the separating surface winding around both rings. Two such concentric tori are visible in all parts of Fig. 9. Outside the separating surface is a similar torus, seen in part (a), (c) and especially (d).

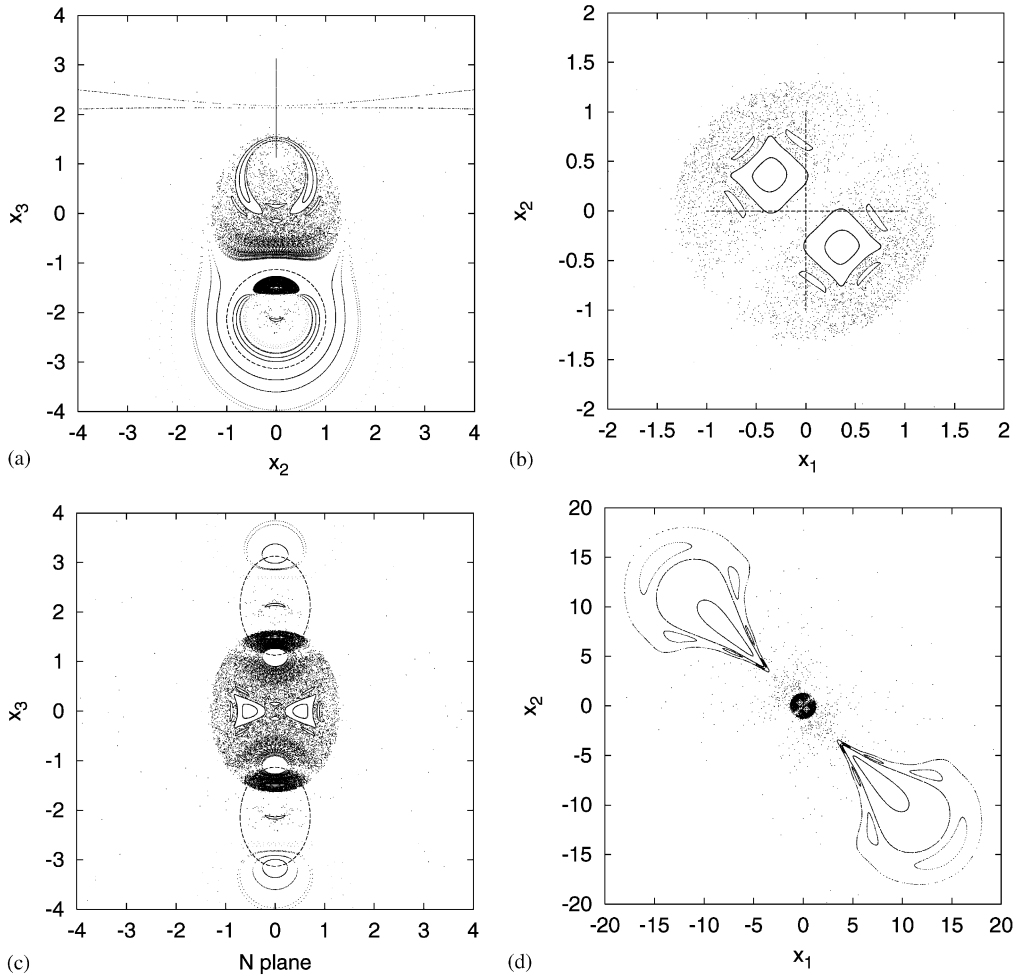


Fig. 9. Poincaré sections for  $d=2.13$ . The “cloud” of points corresponding to chaotic streamlines is contained within a surface. The two concentric tori wind around both rings. The regular islands close to them stem from a single torus that winds around the vortex rings in a more complicated manner. Another torus penetrates close to the ring centers. Not all initial conditions used for part (d) are shown in parts (a) and (c).

Table 2

Location of fixed point at  $(x, x, 0)$  and  $(-x, -x, 0)$  for varying distance between rings. For large distances,  $x$  approaches  $d/2$

$d$	$x$ (approx.)
1	0 (exact)
1.01	0.064
1.1	0.226
2.13	0.944
10	4.976

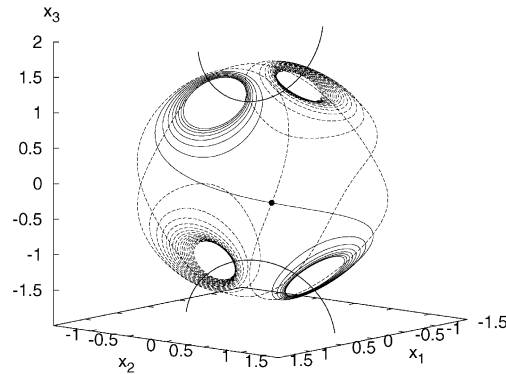


Fig. 10. Unstable (solid line) and stable (dashed line) invariant manifolds of one fixed point on the separating surface for  $d = 2.13$ . The fixed point is marked with  $\bullet$ . Segments of the vortex rings appear as thick lines at the top and bottom. The streamlines lie on a closed surface. The invariant manifolds spiral into a vortex ring, those spots are only left white because of finite integration time. The second fixed point (not shown) has a symmetric set of manifolds.

For large separations,  $d \rightarrow \infty$ , the same qualitative picture holds. The separating surface grows with increasing  $d$  and contains, in the limit, exactly half of each ring. There are always tori going around both rings which necessarily contain periodic streamlines at their center. The size of the tori grows with  $d$  and they form substantial regions of regular streamlines.

Here we emphasize an interesting consequence of the existence of a separating surface. No matter how far apart the two vortex rings are, no regular streamline can wind around one ring only, even arbitrarily close to the ring. The perturbation of the other ring will eventually drag it away from the first ring. This can take an arbitrarily long time, but a closely winded streamline can never go beyond a certain azimuthal position along the vortex ring. Among all ring configurations considered this far, streamlines encircling only one ring are only possible for linked vortex rings.

This ends our exploration of the flow field with different separations  $d$ . A small change in ring positions of the  $d = 0$  configuration can immediately lead to unlinked rings, for example, when the rings are centered at coordinates  $(0, -d', 0)$  and  $(0, d', 0)$  instead of  $(0, 0, \pm d)$ . The remainder of this section briefly discusses the case  $d' = 0.17$ .

The Poincaré section of Fig. 11 shows unbounded chaotic trajectories, a separating surface (the  $x_3 = 0$  plane) and tori that wind around both rings on each side of the separating surface. No regular streamlines wind around one ring only. All this is analogous to our observations in the preceding case. The  $x_3 = 0$  plane is invariant for any  $d'$  and has two hyperbolic fixed points on it. The points where the velocity is perpendicular to the vortex rings are also at  $x_3 = 0$ . The invariant plane hence clearly corresponds to the separating surface discussed above.

This configuration may be considered a perturbation of the  $d = 0$  case. The surface of the double-cone is dissolved and the spiraling trajectories turned chaotic. One can still see in Fig. 11 trajectories that coil along a vortex ring until, closer to the invariant  $x_3 = 0$  plane, they move away from it. The transition to chaos starts again directly from periodic orbits. Unlike the linked configuration of Section 4 the envelope of the double-cone (the separatrix) is immediately dissolved through the displacement of the rings.

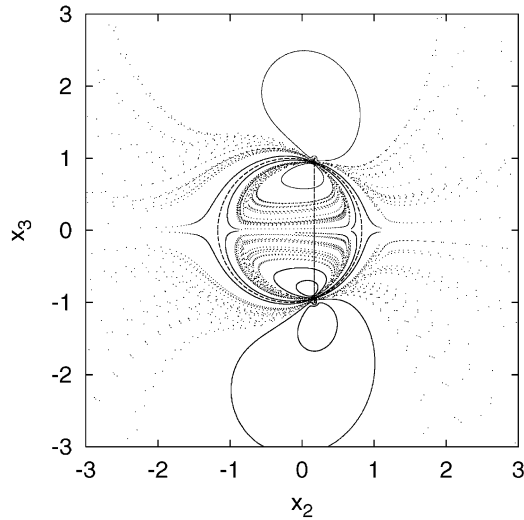


Fig. 11. Poincaré section for  $d' = 0.17$ . The vortex rings are drawn with dashed lines.

This example nicely demonstrates again the generality of the streamline topology as one would expect based on topological equivalence.

## 7. Conclusions and discussion

The main general results found in our study are the following. Two vortex rings can already generate chaotic streamlines (Huang et al., 2000). Chaotic streamlines of two linked vortex rings never extend to infinity. Consequently, motion far away from two linked vortex rings is regular. Motion far away from two unlinked vortex rings can be chaotic. For unlinked vortex rings, a surface separates space into two regions; each vortex ring is part of both regions, and each region contains chaotic and regular streamlines. The global topology of all streamlines is profoundly influenced by the presence of the other ring, no matter how far apart.

The cases where the vortex rings intersect one another are of less general validity and they would furthermore be dynamically highly unstable. Both cases exhibit intertwined stable and unstable invariant manifolds such that the spatial arrangement of topologically distinct streamlines is complex. One of these structures is described in some detail in Section 3, Figs. 2–4.

For  $d = 1$  there is a global bifurcation or heteroclinic bifurcation (Wiggins, 1988), which induces the global variation of topological structures in the flow field. For example, two linked closed orbits can change to unlinked orbits. Another fact, which is indicative of the heteroclinic bifurcation is that when  $d < 1$ , there is only one chaotic region, but when  $d > 1$ , there are two chaotic regions separated by a manifold.

Topological equivalence among flow fields generated by different ring arrangements leads to generalizations of our results. The behavior of the streamlines can be successfully classified according to the topology of the ring configuration: linked, unlinked, with one ring intersection, or two ring intersections. Streamline topologies are similar within the same vortex ring topology and differ vastly for

different vortex ring topologies. A manifestation of this is that the numerical value of the separation  $d$  is unimportant as long as no topological change of the ring configuration takes place.

Elsewhere (Huang et al., 2000) we have, however, pinpointed special cases where streamlines change from periodic to irregular although no ring intersections take place and therefore the ring arrangement remains topologically unchanged. One such special case is two rings that are mirror images of each other. For this configuration no chaotic streamlines arise (Huang et al., 2000). Even streamlines reaching arbitrarily far are regular, although the two rings are unlinked. (Incidentally, we observe in this mirror-symmetric case a manifold structure similar to the double-cone present for  $d=0$ .) This poses the question how robust the streamline topology is with respect to changes in the vortex ring configuration, corresponding to the mathematical concept of structural stability of a three-dimensional vector field. Three-dimensional vector fields are in general not structurally stable (Hirsch and Smale, 1974), but may be structurally stable if the vector field is the gradient of a potential. In our case the velocity field is indeed irrotational, except at the rings where it is singular. We are not aware of any theorem describing structural stability in this situation, if it exists. The aforementioned findings suggest that structural stability, for perturbations corresponding to spatial displacement of rings, is not always the case.

## Acknowledgements

The work of E.S.C.C. and N.S. is supported by a grant from the Research Grants Council of the Hong Kong Special Administrative Region, China (RGC Ref. No. CUHK4119/98P). N.S. also acknowledges a postdoctoral fellowship from the Chinese University of Hong Kong. The work of Y.H. is supported by the National Basic Research Project “Nonlinear Science” and “The several Key Problems of Fluid Mechanics and Aerodynamics”, and also by a Direct Grant of the Chinese University of Hong Kong.

## References

- Aref, H., 1983. Integrable, chaotic and turbulent vortex motion in two-dimensional flows. *Annu. Rev. Fluid Mech.* 15, 345.
- Arnold, V.I., Khesin, B.A., 1998. *Topological Methods in Hydrodynamics*, 2nd Edition. Springer, New York.
- Belin, F., Maurer, J., Tabeling, P., Willaime, H., 1996. Observation of intense filaments in fully developed turbulence. *J. de Phys. II* 6, 573.
- Domon, K., Ishihara, O., Watanabe, S., 2000. Mass transport by a vortex ring. *J. Phys. Soc. Japan* 69, pp. 120.
- Hatakeyama, N., Kambe, T., 1997. Statistical laws of random strained vortices in turbulence. *Phys. Rev. Lett.* 79, 1257.
- He, G.W., Doolen, G.D., Chen, S.Y., 1999. Calculations of longitudinal and transverse velocity structure functions using a vortex model of isotropic turbulence. *Phys. Fluids* 11, 3743.
- Hirsch, M.W., Smale, S., 1974. *Differential Equations, Dynamical Systems, and Linear Algebra*. Academic Press, New York.
- Huang, Y., Schorghofer, N., Ching, E.S.C., 2000. Two vortex rings produce chaos. *Europhys. Lett.* 52, 399.
- Jimenez, J., Wray, A.A., Saffman, P.G., Rogallo, R.S., 1993. The structure of intense vorticity in isotropic turbulence *J. Fluid Mech.*, 255.
- Kambe, T., Hatakeyama, N., 2000. Statistical laws and vortex structures in fully developed turbulence. *Fluid Dyn. Res.* 27, 247.
- Kidambi, R., Newton, P.K., 2000. Streamline topologies for integrable vortex motion on a sphere. *Physica D* 140, 95.

- Kroujiline, D., Stone, H.A., 1999. Chaotic streamlines in steady bounded three-dimensional Stokes flows. *Physica D* 130, 105.
- Lamb, H., 1932. *Hydrodynamics*, 6th Edition. Dover, New York.
- Lugt, H.J., 1983. *Vortex Flow in Nature and Technology*. Wiley, New York.
- Moshier, S.L., 1992. Cephes Mathematical Library. <http://www.netlib.org/cephes/>.
- Neishtadt, A.I., Vainshtein, D.L., Vasiliev, A.A., 1998. Chaotic advection in a cubic Stokes flow. *Physica D* 111, 227.
- Pentek, A., Tel, T., Toroczkai, Z., 1996. Transient chaotic mixing in open hydrodynamical flows. *Int. J. Bifurcat. Chaos* 6, 2619.
- Perry, A.E., Chong, M.S., 1987. A description of eddying motions and flow patterns using critical-point concepts. *Annu. Rev. Fluid Mech.* 19, 157.
- Press, W.H., Teukolsky, S.A., Vetterling, W.T., Flannery, B.P., 1992. *Numerical Recipes in Fortran*, Vol. 1, 2nd Edition. Cambridge University Press, Cambridge, UK.
- Shariff, K., Leonard, A., 1992. Vortex rings. *Annu. Rev. Fluid Mech.* 24, 235.
- Shi, C.C., Huang, Y.N., Zhu, Z.X., Shu, W.D., Deng, Y.F., 1992. Chaotic phenomena produced by the spherical vortices in the beltrami flows. *Chinese Phys. Lett.* 9, 515.
- Stone, H.A., Nadim, A., Strogatz, S.H., 1991. Chaotic streamlines inside drops immersed in steady Stokes flow. *J. Fluid Mech.* 222, 629.
- Vincent, A., Meneguzzi, M., 1991. The spatial structure and statistical properties of homogeneous turbulence. *J. Fluid Mech.* 225, 1.
- Wiggins, S., 1988. *Global Bifurcations and Chaos: Analytical Methods*. Springer, New York.